Water Resources Research

RESEARCH ARTICLE
10.1029/2019WR024771

Key Points:
- Observations indicate that responses of evaporative fraction to heatwaves vary across land cover types
- An analytical attribution method is employed to quantify the relative roles of surface and atmospheric factors
- Heatwave-induced changes in evaporative fraction are mainly caused by changes in vapor pressure deficit and surface resistance

Supporting Information:
- Supporting Information S1

Correspondence to:
D. Li,
lidan@bu.edu

Citation:
Wang, P., Li, D., Liao, W., Rigden, A., & Wang, W. (2019). Contrasting evaporative responses of ecosystems to heatwaves traced to the opposing roles of vapor pressure deficit and surface resistance. *Water Resources Research*, *55*. https://doi.org/10.1029/2019WR024771

Received 14 JAN 2019
Accepted 29 APR 2019
Accepted article online 6 MAY 2019

Contrasting Evaporative Responses of Ecosystems to Heatwaves Traced to the Opposing Roles of Vapor Pressure Deficit and Surface Resistance

Peng Wang[1,2], Dan Li[2], Weilin Liao[3], Angela Rigden[4], and Wen Wang[1]

[1]State Key Laboratory of Hydrology-Water Resources and Hydraulic Engineering, Hohai University, Nanjing, China, [2]Department of Earth and Environment, Boston University, Boston, MA, USA, [3]School of Geography and Planning, Sun Yat-sen University, Guangzhou, China, [4]Department of Earth and Planetary Sciences, Harvard University, Boston, MA, USA

Abstract Understanding the evaporative response of ecosystems to heatwaves is critical for managing ecosystem services and water resources, especially under a changing climate. In this study, we examine the land-atmosphere exchange of water and heat fluxes under heatwave and nonheatwave conditions across five different land cover types, including grasslands, shrublands, croplands, deciduous broadleaf forests, and evergreen needleleaf forests, using data from eddy covariance towers. Results show that net radiation and sensible heat flux increase from nonheatwave to heatwave conditions across all five land cover types but latent heat flux shows contrasting responses to heatwaves. An attribution analysis further demonstrates that heatwave-induced changes in evaporative fraction are mainly caused by changes in vapor pressure deficit (positive contribution) and changes in surface resistance (negative contribution). The imbalance between the positive and negative contributions varies across the five land cover types and is responsible for their contrasting evaporative responses to heatwaves.

Plain Language Summary A heatwave is a period of extremely hot weather. Under a warming climate, heatwaves are expected to become more frequent, stronger, and longer lasting. Heatwaves are amongst the deadliest natural disasters. Within such contexts, key questions that need to be addressed include how different ecosystems respond to heatwaves differently and, more importantly, what factors control such contrasting responses. In this study, we employ an analytical attribution framework and combine it with observational data to explore the responses of evaporative fraction, a key indicator of the partition between sensible and latent heat fluxes, to heatwaves over five major land cover types. We quantify the contributions of various land surface and atmospheric factors in controlling changes in the evaporative fraction under heatwaves. Our analysis indicates that the vapor pressure deficit and surface resistance are the dominant factors but play opposing roles, with changes in the vapor pressure deficit enhancing the evaporative fraction but changes in the surface resistance reducing the evaporative fraction. Their relative contributions vary across land cover types, thereby explaining the contrasting ecosystem responses to heatwaves. By identifying the key factors controlling the ecosystem responses to heatwaves, our results provide novel insights into how to manage ecosystem services and water resources.

1. Introduction

Heatwaves (HWs) are prolonged periods of extremely high temperature typically caused by quasi-stationary high pressure systems (Perkins, 2015). They are amongst the deadliest natural disasters and one of the most important causes of weather-related mortality (Anderson & Bell, 2009, 2011; Harlan et al., 2006; Kovats & Hajat, 2008; Petkova et al., 2014). HWs can also cause widespread ecosystem damages and crop failures (Ciais et al., 2005). Recent examples include the 2003 European HW, the 2010 Russian HW, and the 2015 Pakistan HW.

Observational data indicate that the frequency of HWs has increased over the past few decades (Coumou & Rahmstorf, 2012; Peterson et al., 2013). Many investigations using global climate models find that HWs will become more intense, more frequent, and longer lasting under a warming climate (Lau & Nath, 2012, 2014; Meehl & Tebaldi, 2004). While HWs are typically instigated by the synoptic-scale atmospheric circulation patterns, land-atmosphere feedbacks (Miralles et al., 2018; Seneviratne et al., 2010) have been shown to

strongly influence the local- to regional-scale impacts of HWs (Fischer, Seneviratne, Luthi, & Schar, 2007; Fischer, Seneviratne, Vidale, et al., 2007; Hirschi et al., 2011; Miralles et al., 2014; Santanello et al., 2013; Seneviratne et al., 2006).

The key process governing land-atmosphere feedbacks is the partition of available energy into sensible (H) and latent (LE) heat fluxes (Santanello et al., 2009, 2011, 2018). The partition of available energy into sensible and latent heat fluxes can be characterized by the evaporative fraction (EF), which is defined as the proportion of latent heat flux in the available energy (Gentine et al., 2007), namely,

$$EF = \frac{LE}{H + LE}. \tag{1}$$

Using eddy covariance measurements, previous studies have revealed that different land cover types behave quite differently during HWs. For example, Teuling et al. (2010) found that during the 2003 summer European HW grassland increases evapotranspiration initially, leading to faster soil moisture depletion and thus a critical shift to increased sensible heating. This made grassland a major heating source in the long run, despite that sensible heating was twice as high over forest than over grassland initially. A similar divergence between forests and grasslands was also observed with eddy covariance measurements during the springtime in 2003 over Switzerland (Wolf et al., 2014). Li et al. (2015) compared the flux measurements over an urban site and a rural site and found that in response to the increase of net radiation under HW conditions, the urban site tends to have increased sensible heat flux while the rural site tends to have increased latent heat flux.

The contrasting responses of different land cover types to HWs were also studied using models of various complexities, including idealized convective boundary layer models coupled to land surface parameterizations (Combe et al., 2016; van Heerwaarden & Teuling, 2014), single column models (Stap et al., 2014), and regional and global climate models (Lemordant et al., 2016; Li & Bou-Zeid, 2013). For example, using an idealized land surface-convective boundary layer model, van Heerwaarden and Teuling (2014) demonstrated that the observed divergence in the response of HW conditions between forests and grasslands is largely due to differences in stomatal response to changes in atmospheric temperature and humidity. A recent review paper (Miralles et al., 2018) highlights that HW-induced increases in the vapor pressure deficit, which tend to enhance the atmospheric evaporative demand, will typically reduce stomatal conductance and transpiration under conditions of surface water stress.

While these observational and modeling studies offered great insights into the responses of ecosystems to HWs, an analytical attribution framework for quantifying observed HW-induced changes in EF and their controlling factors remains lacking. In this paper, we extend a recently developed attribution framework (Rigden & Li, 2017) and apply it at eddy covariance sites in the Contiguous United States (CONUS) that span a wide range of climates and land cover types. This attribution framework allows us to identify the key factors causing dissimilarities in the observed evaporative responses to HWs over different land cover types. It can be also used as a diagnostic tool for analyzing model behaviors, thereby providing a new way to understand and constrain complex models.

This paper organized as follows: Section 2 introduces the eddy covariance data and the attribution framework; section 3 presents the main results; section 4 discusses the implications of the findings; and section 5 summarizes the study.

2. Data and Methodology

2.1. Observational Data

We utilize observational data collected at 61 eddy covariance sites in the AmeriFlux network (Figure 1). These sites are spread across the CONUS and represent five major land cover types (grassland or GRA, shrubland or SHB, cropland or CRO, evergreen needleleaf forest or ENF, and deciduous broadleaf forest or DBF). Details about site characteristics and data periods can be found in the supporting information (Table S1 in the supporting information). All AmeriFlux data are obtained from the BASE data product (http://ameriflux.lbl.gov/) and are processed following Rigden and Salvucci (2015).

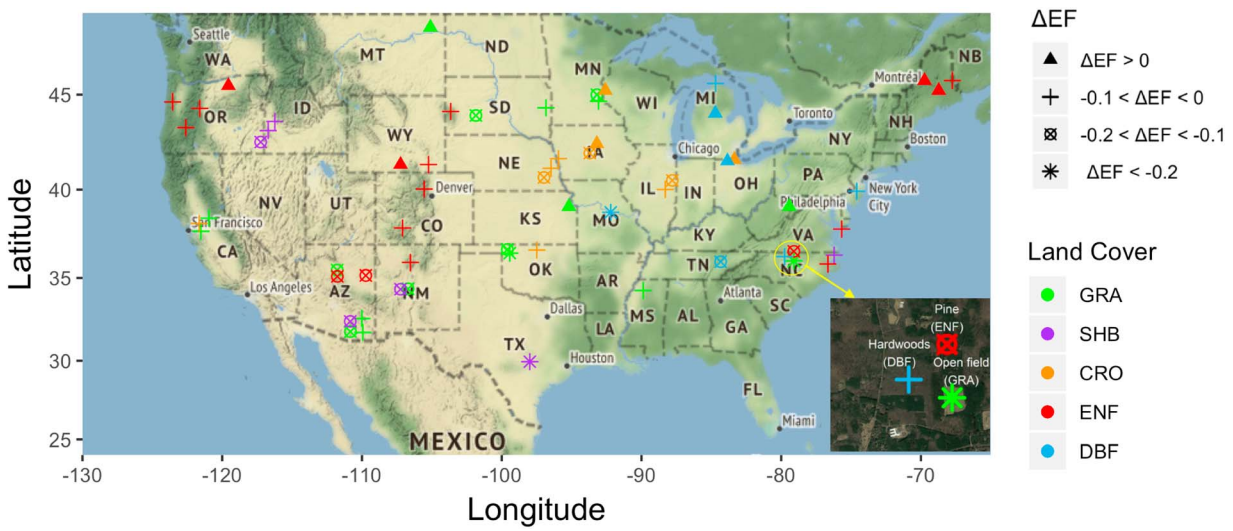

Figure 1. Distribution of 61 AmeriFlux sites across Contiguous United States with different land-cover types, including grassland (GRA, 18 sites), shrubland (SHB, 7 sites), cropland (CRO, 11 sites), deciduous broadleaf forest (DBF, 7 sites), and evergreen needleleaf forest (ENF, 18 sites). Different markers represent different magnitudes of changes in EF between HW and non-HW days. For a few sites, we slightly adjust the coordinates to prevent the symbols from overlapping. The inset highlights the three sites at Duke Forest. EF = evaporative fraction; HW = heatwave.

2.2. Identification of HW Events

We identify HW events based on the locally measured daily maximum air temperature. A HW event is defined as the longest period in which the daily maximum air temperature exceeds its 90th percentile (with a 15-day moving window) for at least 3 days. The 90th percentile is calculated based on all available data at each site. Compared to many studies where the 95th percentile or even the 98th percentile is used (Smith et al., 2013), a less stringent criterion (i.e., the 90th percentile) is used in our study to ensure a sufficiently larger number of HW days and enough data under HW conditions. The number of HW days and non-HW days at each site can be also found in the supporting information (Table S1).

2.3. The Attribution Method

We employ an analytical method to attribute changes in EF into various atmospheric and land surface drivers. This attribution method builds upon the recently proposed Two-Resistance Mechanism (TRM) method (Rigden & Li, 2017). The TRM model starts from the surface energy balance equation:

$$R_n = S_{in}(1-\alpha) + \varepsilon L_{in} - \varepsilon\sigma T_s^4 = H + LE + G, \tag{2}$$

where R_n is the net radiation; S_{in} and L_{in} are the incoming shortwave and longwave radiation, respectively; α and ε are the albedo and emissivity, respectively; $\varepsilon\sigma T_s^4$ is the outgoing longwave radiation ($= L_{out}$) where σ is the Stefan-Boltzmann constant and T_s is the land surface temperature; H and LE are the sensible and latent heat fluxes, respectively; G is the ground heat flux. Further connecting H and LE with T_s through the aerodynamic resistance (r_a) and surface or canopy resistance (r_s) concepts (Brutsaert, 1982, 2005; Monteith & Unsworth, 2008) gives

$$H = \frac{\rho c_p}{r_a}(T_s - T_a) \tag{3}$$

$$LE = \frac{\rho L_v}{r_a + r_s}\left(q_s^*(T_s) - q_a\right) \tag{4}$$

where ρ is the air density, c_p is the specific heat of air at constant pressure, L_v is the latent heat of vaporization, T_a is the air temperature, and q_a is the specific humidity of air. It should be pointed out that when vegetation and soil coexist, r_s is the single, big leaf type of surface resistance (Monteith & Unsworth, 2008). Substituting equations (3) and (4) into equation (2) yields a nonlinear equation for T_s, with all other variables treated as inputs. This equation is further linearized, as shown in Rigden and Li (2017), so that an analytical

Table 1
Sensitivities of Evaporative Fraction to Changes in Atmospheric and Surface Factors

	$\frac{\partial EF}{\partial T_a}$ (K^{-1})	$\frac{\partial EF}{\partial P}$ $(P_a{}^{-1})$	$\frac{\partial EF}{\partial S_{in}}$ (m^2/W)	$\frac{\partial EF}{\partial L_{in}}$ (m^2/W)	$\frac{\partial EF}{\partial VPD}$ $(P_a{}^{-1})$	$\frac{\partial EF}{\partial r_a}$ (m/s)	$\frac{\partial EF}{\partial r_s}$ (m/s)	$\frac{\partial EF}{\partial \alpha}$ $(-)$	$\frac{\partial EF}{\partial G}$ (m^2/W)
GRA	7.3×10^{-3}	-1.25×10^{-6}	-4.28×10^{-4}	-4.78×10^{-4}	6.21×10^{-5}	1.70×10^{-3}	-5.89×10^{-4}	3.62×10^{-1}	5.19×10^{-4}
SHB	6.2×10^{-3}	-1.08×10^{-6}	-4.45×10^{-4}	-4.88×10^{-4}	5.58×10^{-5}	2.10×10^{-3}	-5.07×10^{-4}	3.47×10^{-1}	5.25×10^{-4}
CRO	8.3×10^{-3}	-1.29×10^{-6}	-5.11×10^{-4}	-5.76×10^{-4}	9.03×10^{-5}	2.00×10^{-3}	-9.85×10^{-4}	4.64×10^{-1}	6.26×10^{-4}
ENF	6.1×10^{-3}	-9.61×10^{-7}	-5.04×10^{-4}	-5.28×10^{-4}	1.02×10^{-4}	4.3×10^{-3}	-1.00×10^{-3}	4.03×10^{-1}	5.56×10^{-4}
DBF	7.5×10^{-3}	-8.71×10^{-7}	-6.79×10^{-4}	-7.33×10^{-4}	2.01×10^{-4}	4.5×10^{-3}	-1.80×10^{-3}	4.89×10^{-1}	7.89×10^{-4}

Note. EF = evaporative fraction; VPD = vapor pressure deficit.

expression for T_s can be obtained, which further yields analytical expressions for the sensible and latent heat fluxes and thus the EF.

Previous applications of this TRM method were limited to analyzing land surface temperature or EF changes induced only by changes in surface biophysical factors (i.e., the atmosphere conditions remain unchanged). Under such conditions, one can use this model to attribute changes in EF to contributions from various surface biophysical factors, including aerodynamic resistance, surface resistance, albedo, and ground heat flux, as follows:

$$\Delta EF = \left(\frac{\partial EF}{\partial r_a}\right)\Delta r_a + \left(\frac{\partial EF}{\partial r_s}\right)\Delta r_s + \left(\frac{\partial EF}{\partial \alpha}\right)\Delta\alpha + \left(\frac{\partial EF}{\partial G}\right)\Delta G \tag{5}$$

where Δ indicates a change (e.g., induced by land-use/land-cover change such as deforestation and urbanization). The partial derivatives represent the sensitivities of EF to changes in surface biophysical factors, whose analytical formulations can be obtained from the analytical expression for EF. This is similar to the analytical formulations for the sensitivities of land surface temperature, which can be found in Rigden and Li (2017).

In the case of HWs, however, changes in EF are not only caused by changes in surface biophysical factors but also changes in atmospheric conditions. To incorporate the effects of both land surface and atmospheric changes, we build on the TRM method, such that changes in EF can be attributed to

$$\begin{aligned}\Delta EF = &\left(\frac{\partial EF}{\partial T_a}\right)\Delta T_a + \left(\frac{\partial EF}{\partial P}\right)\Delta P + \left(\frac{\partial EF}{\partial S_{in}}\right)\Delta S_{in} + \left(\frac{\partial EF}{\partial L_{in}}\right)\Delta L_{in} + \left(\frac{\partial EF}{\partial VPD}\right)\Delta VPD + \left(\frac{\partial EF}{\partial r_a}\right)\Delta r_a \\ &+ \left(\frac{\partial EF}{\partial r_s}\right)\Delta r_s + \left(\frac{\partial EF}{\partial \alpha}\right)\Delta\alpha + \left(\frac{\partial EF}{\partial G}\right)\Delta G\end{aligned} \tag{6}$$

In addition to accounting for changes in aerodynamic resistance, surface resistance, albedo, and ground heat flux, as in the original TRM method in equation (5), the improved attribution framework in equation (6) also takes into account changes in air temperature (T_a), pressure (P), incoming shortwave radiation (S_{in}), incoming longwave radiation (L_{in}), and vapor pressure deficit (VPD, defined as $e_s^*(T_a) - e_a$ where $e_s^*(T_a)$ is the saturated water vapor pressure at T_a, and e_a is the water vapor pressure). By including these extra attribution variables, the new method provides insight into how changes in land surface conditions (such as surface resistance) would amplify or hinder local changes in EF concomitant with effects originating from changes in atmospheric conditions, such as changes in the air temperature. Throughout the paper, each term on the right-hand side of equation (6) will be called a "contribution." Each contribution is composed of two parts: the partial derivative (or the "sensitivity," Table 1) and the change (Table 2).

2.4. Application of the Attribution Method to Observational Data

The application of the attribution method closely follows the studies by Liao et al. (2018) and Li et al. (2019), in which the TRM method was applied to attribute the local surface temperature response to deforestation and urbanization, respectively. We refer the reader to Liao et al. (2018) and Li et al. (2019) for a detailed description of the methodology and summarize only key details below.

Table 2
Changes in Atmospheric and Surface Factors Between HW and Non-HW Days

	ΔT_a (K)	ΔP (P_a)	ΔS_{in} (W/m^2)	ΔL_{in} (W/m^2)	ΔVPD (P_a)	Δr_a (s/m)	Δr_s (s/m)	$\Delta\alpha$ $(-)$	ΔG (W/m^2)
GRA	7.26	-1.40×10^{2}	1.58×10^{2}	2.61×10^{1}	3.58×10^{3}	-3.86	1.28×10^{3}	-8.00×10^{-3}	4.16×10^{1}
SHB	6.39	3.20×10^{1}	1.42×10^{2}	1.93×10^{1}	3.34×10^{2}	-1.17×10^{-1}	1.42×10^{3}	5.20×10^{-3}	3.48×10^{1}
CRO	7.34	-7.88×10^{1}	1.47×10^{2}	3.53×10^{1}	2.04×10^{2}	1.33	2.45×10^{2}	2.00×10^{-3}	4.47×10^{1}
ENF	6.77	5.57×10^{1}	1.56×10^{2}	2.25×10^{1}	1.69×10^{3}	9.60×10^{-1}	2.13×10^{2}	-5.80×10^{-3}	2.69×10^{1}
DBF	6.61	5.22×10^{1}	1.42×10^{2}	3.25×10^{1}	1.21×10^{2}	-7.59×10^{-2}	1.91×10^{2}	-7.30×10^{-3}	3.95×10^{1}

First, one common issue across eddy covariance sites is that the sum of sensible and latent heat fluxes is smaller than the difference between net radiation and ground heat flux, which is often called the surface energy imbalance or nonclosure problem (see Foken, 2008 for a review). While addressing the causes of the surface energy imbalance problem is beyond the scope of this study, we need to account for such imbalance when we apply the attribution method to eddy covariance data. This is because the attribution method is based on the surface energy balance equation. To do so, we denote $r = R_n - H - LE - G$ as the residual term arising from the use of eddy covariance observations. With this residual term, equation (6) now becomes

$$\Delta EF = \left(\frac{\partial EF}{\partial T_a}\right)\Delta T_a + \left(\frac{\partial EF}{\partial P}\right)\Delta P + \left(\frac{\partial EF}{\partial S_{in}}\right)\Delta S_{in} + \left(\frac{\partial EF}{\partial L_{in}}\right)\Delta L_{in} + \left(\frac{\partial EF}{\partial VPD}\right)\Delta VPD + \left(\frac{\partial EF}{\partial r_a}\right)\Delta r_a + \left(\frac{\partial EF}{\partial r_s}\right)\Delta r_s + \left(\frac{\partial EF}{\partial \alpha}\right)\Delta\alpha + \left(\frac{\partial EF}{\partial (G+r)}\right)\Delta(G+r) \quad (7)$$

Given that many sites do not have ground heat flux measurements, we further combine the contributions of r and G and denote the sum as *res*. Thus,

$$\Delta EF = \left(\frac{\partial EF}{\partial T_a}\right)\Delta T_a + \left(\frac{\partial EF}{\partial P}\right)\Delta P + \left(\frac{\partial EF}{\partial S_{in}}\right)\Delta S_{in} + \left(\frac{\partial EF}{\partial L_{in}}\right)\Delta L_{in} + \left(\frac{\partial EF}{\partial VPD}\right)\Delta VPD + \left(\frac{\partial EF}{\partial r_a}\right)\Delta r_a + \left(\frac{\partial EF}{\partial r_s}\right)\Delta r_s + \left(\frac{\partial EF}{\partial \alpha}\right)\Delta\alpha + \left(\frac{\partial EF}{\partial res}\right)\Delta res \quad (8)$$

where the contribution of *res* reflects the roles of ground heat flux and surface energy imbalance. We acknowledge that at places where ground heat flux measurements do exist, we can correct the r term by partitioning it into H and LE, assuming that the ratio of H to LE remains the same. We find that this correction does not affect the attribution results much because, as shall be seen later, the contribution of *res* is very small, which further implies that our main conclusions will not be strongly affected by the way G and r are handled.

Second, in order to retrieve T_s from outgoing longwave radiation measurements, we assume constant emissivity values of 0.92, 0.93, 0.92, 0.95, and 0.93 for grassland, cropland, shrubland, evergreen needleleaf forest, and deciduous broadleaf forest, respectively (Tao et al., 2013). The estimated T_s, together with the flux and meteorological measurements, serve as inputs to estimate the aerodynamic resistance and surface resistance using equations (3) and (4) at the half-hourly scale.

Third, we only focus on the 6-hr period (9:00–15:00, local standard time) during daytime when sensible heating from the surface is largest. We exclude the half-hourly data when the inferred aerodynamic resistance, surface resistance, or vapor pressure deficit are negative. We also exclude the half-hourly data when any one of the required variables in the attribution analysis is missing. Furthermore, we also exclude the data when the latent heat flux and/or sensible heat flux are less than 20 W/m^2. To ensure data representativeness, for each day, we require at least 50% of the data points in the 6-hr period which are available. We then average the half-hourly data in this 6-hr period under HW and non-HW conditions to compute the changes (Δ) between HW and non-HW conditions.

Lastly, the attribution method only retains the first-order linear terms, neglecting higher-order and cross-order terms in the Taylor expansion. This will inevitably introduce errors in the attribution. To reduce

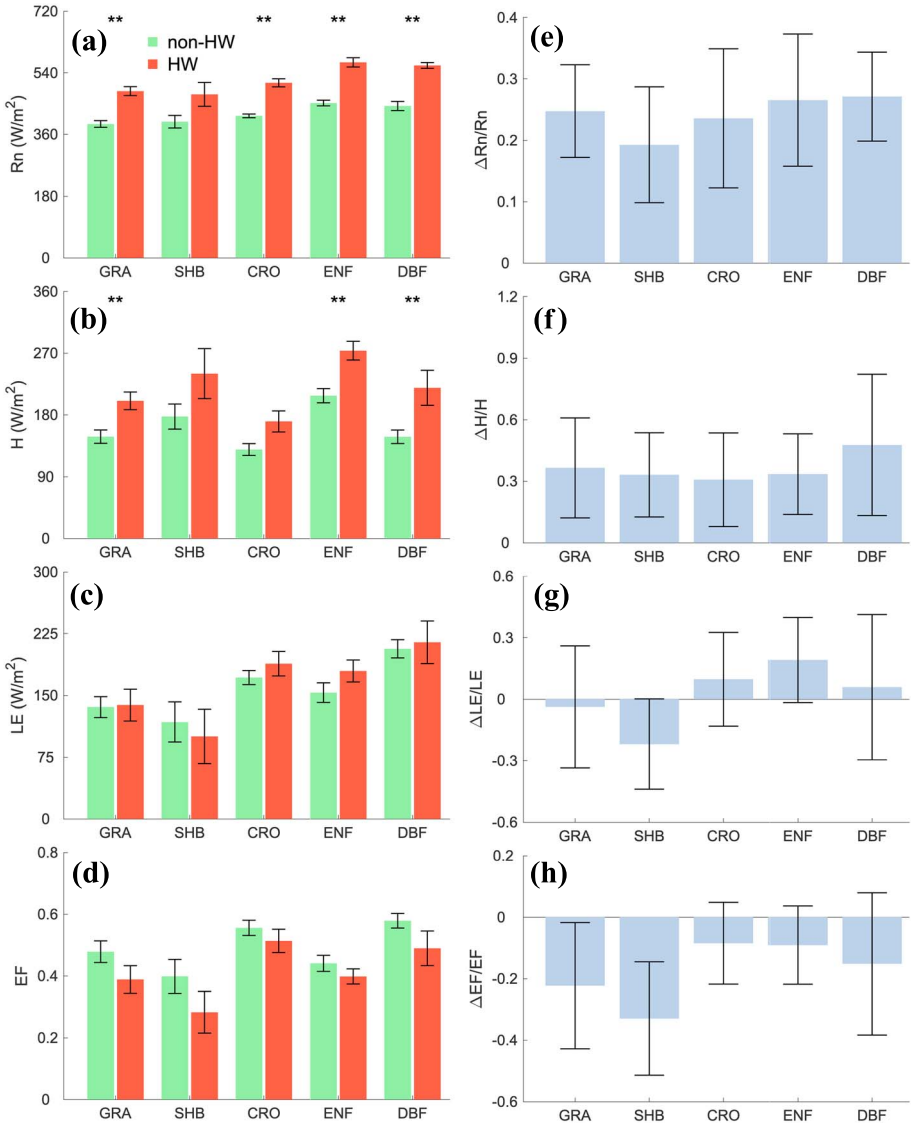

Figure 2. The average (a) net radiation, (b) sensible heat flux, (c) latent heat flux, (d) evaporative fraction under HW and non-HW days over different land cover types, and the corresponding relative (fractional) changes in net radiation (e), sensible heat flux (f), latent heat flux (g), and evaporation fraction (h) between HW and non-HW days. The bars are averages over all sites that have the same land cover type. The error bars in (a–d) represent the standard deviations of the averages, and those in (e–h) represent the standard deviations. All error bars characterize the spatial variability across sites. The ** indicates that the averages in HW and non-HW days are significantly different at the 95% confidence level in paired sample *t* test.

such errors, a weighted approach is introduced (Liao et al., 2018), which calculates the partial derivatives (or the sensitivities) based on data at both states (i.e., the HW and non-HW states) as $X = (x_{non\ -\ hw}+mx_{hw})/(1+m)$,where X is the final partial derivative in the model, m is average weight, and x_{hw} and $x_{non\text{-}hw}$ are the partial derivatives calculated only using data under HW and non-HW conditions, respectively. More details can be found in Liao et al. (2018).

3. Results

3.1. Evaporative Responses of Ecosystems to HWs Across CONUS

For all five land cover types, we find that the average net radiation (Figure 2a) is significantly higher during HWs, implying that the ecosystems receive more radiation input during HWs. This is consistent with the fact

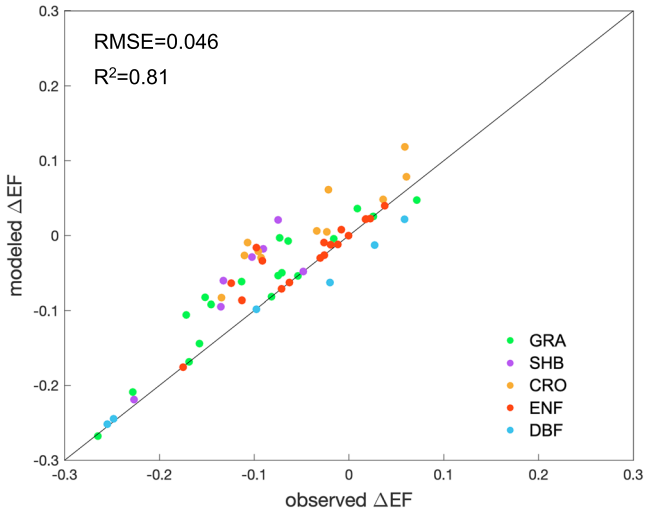

Figure 3. Comparison between the modeled and observed mean ΔEF. EF = evaporative fraction; RMSE = root-mean-square error.

that HWs are typically associated with clear, cloudless sky (Perkins, 2015). The partition of net radiation to sensible and latent heat is also strongly altered by HWs. On average the sensible heat flux increases across all five land cover types (Figure 2b), while the latent heat flux shows contrasting responses to HWs: It decreases over shrublands, barely changes over grasslands and deciduous broadleaf forests, but increases over croplands and evergreen needleleaf forests (Figure 2c). This causes stronger reductions of EF at shrublands, grasslands, and deciduous broadleaf forest sites than cropland and evergreen needleleaf forest sites (Figure 2d).

The strongest reduction of latent heat flux over shrubland ecosystems may reflect the fact that shrublands tend to grow in more water-limited regions and, thus, likely have more depleted moisture reserves in the root zone, especially compared to forests. On the other hand, the increase of latent heat flux over cropland systems may be related to irrigation (Miralles et al., 2018). We caution that there are large spatial variabilities associated with changes in EF even over the same land cover type though (see Figures 1 and 2d), which can be caused by other factors including species, soil types, and background climates (De Kauwe et al., 2015; Konings et al., 2017), as well as rooting depth and access to groundwater (Bevan et al., 2014; Thompson et al., 2011), but such factors are difficult to quantify and left for future research. In addition, we point out that changes in LE and EF are not significant at the 95% confidence level.

3.2. Attribution of the Evaporative Response to HWs

To further investigate why different ecosystems have different evaporative responses to HWs, we employ an attribution method by extending the TRM model (section 2.3). First, we evaluate changes in EF estimated by the TRM method, finding good agreement between modeled and observed changes, as illustrated in Figure 3. The remaining biases can be attributed to the inadequacy of the weighted approach (Liao et al., 2018) in accounting for the neglected higher-order and cross-order terms in the Taylor expansion and the measurement uncertainties when sensible and latent heat fluxes are small.

Changes in EF from non-HW to HW days are then decomposed to contributions from five atmospheric factors (e.g., air temperature, pressure, incoming shortwave radiation, incoming longwave radiation, and vapor pressure deficit) and four land surface factors (e.g., aerodynamic resistance, surface resistance, surface albedo, and residual), as shown in Figure 4. Part I of Figure 4 again indicates the good agreement between the modeled and observed ΔEF, where the error bars again indicate strong spatial variabilities (see also Figure 2d). When the contributions from atmospheric and land surface components are aggregated, we find that the total atmospheric contribution (f_a) and the total land surface contribution (f_s) are always opposite. More specifically, the total atmospheric contributions (f_a) are always positive and the total land surface contributions (f_s) are always negative (part II of Figure 4). This suggests that under HWs, changes in the atmospheric conditions tend to increase the EF while the land surface responses tend to constrain or limit the EF. Although the total land surface contributions are always larger in magnitude than the total atmospheric contributions, the five land cover types show distinct responses, leading to EF changes of different magnitudes.

When each atmospheric factor is assessed individually (part III of Figure 4, blue bars), we find that changes in VPD make the largest positive contribution (i.e., increases in VPD tend to increase the EF), whereas changes in the incoming shortwave and longwave radiation consistently make negative contributions (i.e., increases in incoming shortwave and longwave radiation tend to reduce the EF by favoring sensible heat flux) across all land cover types. The negative contributions of incoming shortwave and longwave radiation are largely offset by the positive contribution of air temperature, which is the second largest positive condition (i.e., increases in air temperature tend to increase the EF). Thus, VPD is the dominant atmospheric factor in regulating the EF response to HWs. Note that changes in pressure make minimal contributions.

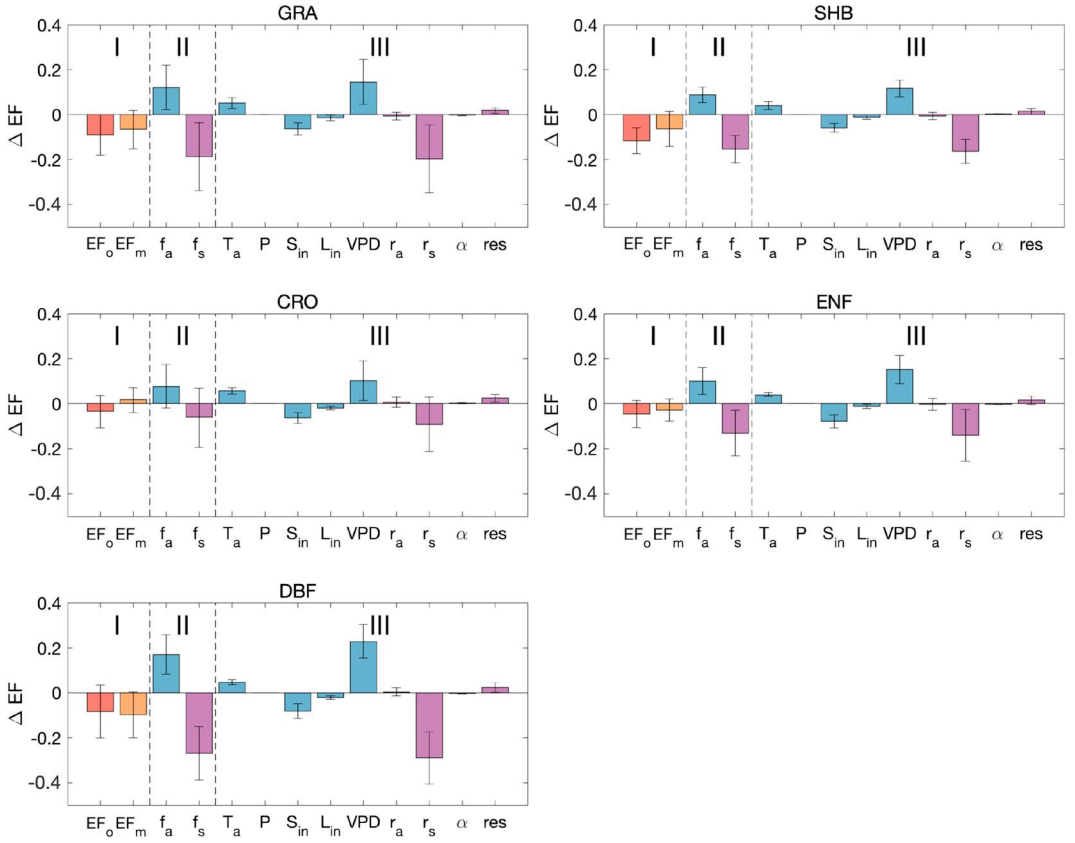

Figure 4. Attribution of changes in evaporative fraction (ΔEF) between HW and non-HW days at AmeriFlux sites with different land cover types. Part I: Comparison of observed and modeled EF changes. EF_o and EF_m represents the observed and modeled evaporative fraction changes from non-HW to HW days. Part II: Comparison of the total atmospheric (f_a) and land surface (f_s) contributions. Part III: Contribution from each atmospheric (blue bar) and land surface (purple bar) factor (i.e.,$(\partial EF/\partial x_i)\Delta x_i$, where x_i is a factor). T_a, P, S_{in}, L_{in}, VPD, r_a, r_s, α, and res represent air temperature, pressure, incoming shortwave radiation, incoming longwave radiation, vapor pressure deficit, aerodynamic resistance, surface resistance, albedo, and residual, respectively. EF = evaporative fraction.

Among the surface factors (part III of Figure 4, purple bars), the surface resistance makes the strongest negative contribution (i.e., increases in the surface resistance tend to reduce the EF). This is consistent with previous studies suggesting that plants tend to close their stomata under heat and drought stresses, thereby increasing the surface resistance (Damour et al., 2010; Jones, 2014). Broadly, stomata close in response to declines in soil moisture to prevent hydraulic damage such as cavitation (Tyree & Sperry, 1989), while stomatal closure induced by high VPD prevents both excessive water loss in the root zone and hydraulic damage (Oren et al., 1999). Additionally, reductions in near-surface soil moisture under HW conditions would also increase the surface resistance. The other terms, including the residual term, all make small contributions.

The small contributions from pressure and albedo are due to the very small sensitivity of EF to pressure and the very small change of albedo, respectively, as seen in Table 1 and Table 2. On the other hand, the large contributions from VPD and surface resistance are caused by the significant increases in VPD and surface resistance under HWs. The contributions from the other factors, including air temperature, aerodynamic resistance, incoming shortwave and longwave radiation, and residual, are of the same order of magnitude. The sensitivities of EF to changes in air temperature and aerodynamic resistance are an order of magnitude larger than the sensitivities of EF to changes in incoming shortwave radiation, incoming longwave radiation, and residual. However, changes in air temperature and aerodynamic resistance are an order of magnitude smaller than their counterparts in incoming shortwave radiation, incoming longwave radiation, and residual. Hence, the contributions from air temperature, aerodynamic resistance, incoming shortwave radiation, incoming longwave radiation, and residual are of the same order of magnitude.

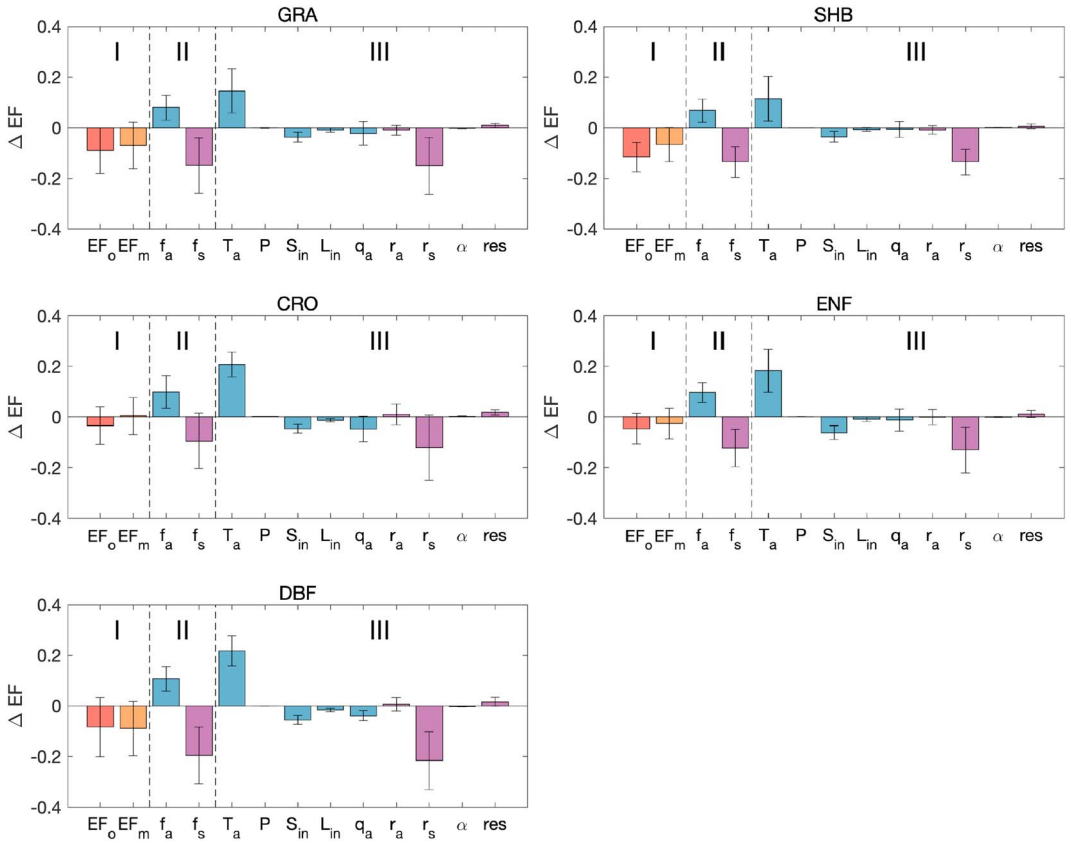

Figure 5. Similar to Figure 4 but using q_a instead of VPD. EF = evaporative fraction.

4. Discussions

As shown in Figure 4, HWs alter the EF largely through VPD and surface resistance. In this section, we discuss the opposing roles of these two factors in the context of the surface energy balance equation.

4.1. VPD

In our attribution method, VPD appears in the parameterization of latent heat flux (equation (4)) after the linearization of the saturated specific humidity (or vapor pressure). Since VPD is dependent on air temperature and specific humidity, we further decompose the contribution of VPD into air temperature and specific humidity components, as shown in Figure 5.

With this decomposition of VPD, we find that the contribution of air temperature to changes in EF is significantly increased and becomes the largest positive term. This indicates that the large contribution from VPD is mostly a result of the increased air temperature. On the other hand, the contribution of specific humidity is mostly negative, implying that increases in specific humidity under HWs tend to reduce the EF (as expected). While both attribution results are correct, their differences, especially the difference in terms of the contribution of air temperature, illustrate a broader but often neglected issue in such attribution analyses, that is, the interdependence of attributing variables (Rigden & Li, 2017). Since VPD and air temperature are by definition linked to each other, the contribution of air temperature will change, for example, when specific humidity is used to replace VPD as an attributing variable. Nonetheless, we use VPD as an attributing variable here as it is often used as a single variable in the literature (Brutsaert, 1982). In fact, recent studies using spectral analysis show that treating VPD as a single variable better captures the temporal dynamics of atmospheric evaporative demand than using a combination of air temperature and specific or relative humidity (Peng et al., 2018).

Under HW conditions, an increase of VPD would lead to an increase of atmospheric evaporative demand. Clearly this effect alone would increase evapotranspiration and hence the EF, as the attribution results suggest (Figure 4). However, evapotranspiration over a vegetated surface is also constrained by soil moisture (for

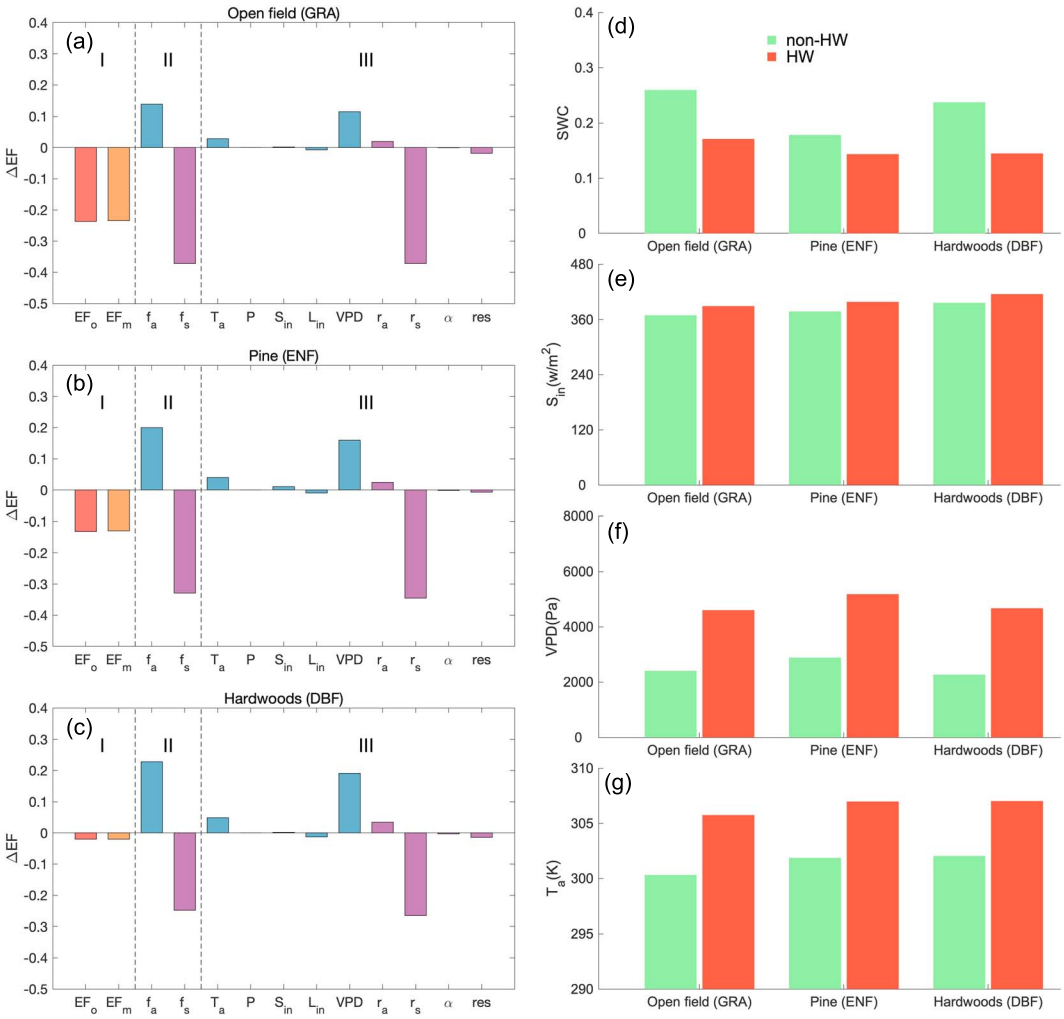

Figure 6. (a–c) Similar to Figure 4. Attribution of changes in EF between HW and non-HW days at three Duke sites (open field/GRA, pine/ENF, and hardwoods/DBF). (d–g) Similar to Figure 2. The average (d) soil water content (SWC), (e) incoming shortwave radiation, (f) vapor pressure deficit, and (g) air temperature under HW and non-HW days over the three Duke sites. The soil moisture measurement depths at open field/GRA, pine/ENF, and hardwoods/DBF sites are 25, 30, and 25 cm, respectively. EF = evaporative fraction; HW = heatwave; VPD = vapor pressure deficit.

soil evaporation) and stomatal behavior (for transpiration). The role of these factors in the surface energy balance equation is reflected in the contribution of surface resistance, which is further discussed below.

4.2. Surface Resistance

As shown in Figure 4, the surface resistance makes the largest negative contribution to HW-induced EF changes. Given that the surface resistance is a bulk parameter, this implies that under HWs (1) available water for evapotranspiration (including soil moisture, intercepted water on canopy surfaces, and puddles on the ground) is reduced, (2) plants close their stomata or the leaf area index (LAI) is reduced, or (3) a combination of both. Since not all AmeriFlux sites have soil moisture measurements, here we use three neighboring sites at Duke Forest (hereafter the Duke sites; see Figure 1), which sites have soil moisture measurements at 25–30 cm under the ground and are over different land cover types (open field/GRA, pine/ENF, and hardwoods/DBF), as a case study.

Before we proceed, it is important to examine the attribution results at these three sites, as shown in Figures 6a–6c. It is clear that reductions in EF are the strongest at the open field (GRA) site and the smallest at the hardwoods (DBF) site. The stronger reduction of EF at the ENF site than that at the DBF site may at first appear to be inconsistent with the results shown in Figure 2, but we again point out that there are large

spatial variabilities associated with changes in EF across sites (see Figure 1). At the Duke sites, the VPD and surface resistance make the largest positive and negative contributions, which is in agreement with Figure 4.

Under HW conditions, soil moisture is likely to be depleted as a result of increased evapotranspiration and the lack of rain. This is confirmed by Figure 6d. At all three Duke sites, soil moisture decreases during HWs. Since drier soils have higher resistances to evaporation, this decline in soil moisture during HWs likely increases the total effective surface resistance.

While soil evaporation is a purely physical process, transpiration is biologically mediated. Plants actively respond to changes in environmental conditions by changing their stomatal aperture and, thus, changing the effective surface resistance. One way to parameterize the stomatal resistance is the so-called Jarvis scheme (Jarvis, 1976; Stewart, 1988) as follows:

$$r_s = \frac{r_{s,\min}}{LAI} f_1(\mathrm{SWC}) f_2(S_{in}) f_3(\mathrm{VPD}) f_4(T_a) \tag{9}$$

where $r_{s,min}$ is the minimal stomatal resistance, LAI is the leaf are index, and f_n are correction functions accounting for the effects of soil water content (SWC), incoming shortwave radiation (S_{in}), VPD, and air temperature (T_a). It is important to recognize that decreases in soil moisture can both increase the resistance of soil (decreasing soil evaporation) and induce stomatal closure (decreasing transpiration), with the near-surface soil moisture more strongly linked to the soil resistance while the root zone soil moisture more strongly linked to the stomatal resistance.

The functions for f_n are empirical and often site dependent, but generally, the surface resistance increases as the root zone soil moisture and incoming shortwave radiation decrease, and as the VPD increases (Jones, 2014). When the air temperature is above a certain threshold (typically 298 K but can be species dependent), the stomatal resistance also increases as the air temperature increases. Under HW conditions, the incoming shortwave radiation, VPD, and air temperature all increase (and the air temperature is far above 298 K), while the soil moisture decreases (see Figures 6d–6g). As a result, changes in VPD, air temperature, and soil moisture are all likely leading to increases in stomatal resistance, which limits transpiration and thus the EF.

4.3. The Dual Role of VPD

Our results suggest that VPD plays a dual role in controlling the evaporative responses of land ecosystems to HWs. While an increase in VPD tends to increase the atmospheric evaporative demand, it can also lead to an increase in surface resistance, which tends to inhibit evapotranspiration (Ficklin & Novick, 2017; Massmann et al., 2018; Novick et al., 2016). An unanswered question in our study is exactly what role VPD plays in modulating the response of surface resistance to HWs.

More broadly, our attribution analysis does not explain which factor (e.g., VPD or soil moisture) is mostly responsible for the response of surface resistance to HWs. Disentangling the effects of atmospheric demand (represented by VPD) and soil moisture supply on surface resistance and thus evapotranspiration remains a grand challenge as discussed elsewhere (Novick et al., 2016; Rigden et al., 2018). To analytically attribute changes in surface resistance, this would require, at least, a priori knowledge of the functions in the Jarvis formulation (equation (9)) and how these functions differ among ecosystems. However, these functions are empirical and often vary depending on site-specific factors. While one might be tempted to constrain the Jarvis parameterization and the associated f_n functions through a tuning exercise, a unique solution does not necessarily exist (Bonan et al., 2014; van Heerwaarden & Teuling, 2014). Fully addressing this question is left for future research.

5. Conclusions and Future Work

In this study, we employ an analytical attribution framework to quantify the evaporative responses of ecosystems to HWs. The attribution model is applied to 61 AmeriFlux sites that span five major land cover types. It is found that the VPD and surface resistance are the most important atmospheric and land surface factors, respectively, in controlling the changes in EF under HWs. The reductions in the EF under HWs are driven by the contributions from surface resistance, partly offset by the contributions from VPD. The imbalance between the positive and negative contributions varies across land ecosystems and is responsible for the overall contrasting evaporative responses to HWs.

A critical question remaining to be addressed is what factors regulate the bulk surface resistance response to HWs. This requires a quantitative understanding of how the bulk surface resistance is controlled by environmental variables. Another question that needs to be further investigated is the spatial variability of HW-induced EF changes over the same land cover type. For example, the Duke hardwoods (DBF) site shows smaller reductions in EF than the pine (ENF) site, although DBF sites on average show larger reductions in EF than ENF sites across the CONUS. This might be due to variations in the local land surface (e.g., soil properties) and climate conditions, as well as species. However, it should be stressed that despite of the large spatial variability, the contrasting evaporative responses of ecosystems to HWs are always traced to the opposing roles of vapor pressure deficit and surface resistance in the attribution. Lastly, we did not examine the temporal dynamics of EF throughout HWs but it is important to acknowledge that the temporal dynamics of EF can be very different between grasslands and forests especially under very long HWs (Teuling et al., 2010).

Acknowledgments
We thank the AmeriFlux primary investigators of the sites used in this study. AmeriFlux data are available at http://ameriflux.lbl.gov website. We thank Dr. Adriaan J. Teuling and two other reviewers whose comments led to significant improvement of the quality of the paper. P. W. and W. W. acknowledge financial support from 111 Project (no. B08048), Fundamental Research Funds for the Central Universities (no. 2017B614X14), and Postgraduate Research and Practice Innovation Program of Jiangsu Province (no. KYCX17_0419). This material is based upon work supported by the US Army Research Office under Grant No. W911NF-18-1-0360. This work was conducted when the first author visited Boston University in 2017–2018.

References

Anderson, B. G., & Bell, M. L. (2009). Weather-related mortality: How heat, cold, and heat waves affect mortality in the United States. *Epidemiology*, *20*(2), 205–213. https://doi.org/10.1097/EDE.0b013e318190ee08

Anderson, B. G., & Bell, M. L. (2011). Heat waves in the United States: Mortality risk during heat waves and effect modification by heat wave characteristics in 43 U.S. communities. *Environmental Health Perspectives*, *119*(2), 210–218. https://doi.org/10.1289/ehp.1002313

Bevan, S. L., Los, S. O., & North, P. R. J. (2014). Response of vegetation to the 2003 European drought was mitigated by height. *Biogeosciences*, *11*(11), 2897–2908. https://doi.org/10.5194/bg-11-2897-2014

Bonan, G. B., Williams, M., Fisher, R. A., & Oleson, K. W. (2014). Modeling stomatal conductance in the earth system: Linking leaf water-use efficiency and water transport along the soil-plant-atmosphere continuum. *Geoscientific Model Development*, *7*(5), 2193–2222. https://doi.org/10.5194/gmd-7-2193-2014

Brutsaert, W. (1982). *Evaporation into the atmosphere: Theory, history, and applications* (299 pp.). Dordrecht, Holland: Reidel.

Brutsaert, W. (2005). *Hydrology: An introduction* (605 pp.). New York: Cambridge University Press. https://doi.org/10.1017/CBO9780511808470

Ciais, P., Reichstein, M., Viovy, N., Granier, A., Ogée, J., Allard, V., et al. (2005). Europe-wide reduction in primary productivity caused by the heat and drought in 2003. *Nature*, *437*(7058), 529–533. https://doi.org/10.1038/nature03972

Combe, M., de Arellano, J. V. G., Ouwersloot, H. G., & Peters, W. (2016). Plant water-stress parameterization determines the strength of land-atmosphere coupling. *Agricultural and Forest Meteorology*, *217*, 61–73. https://doi.org/10.1016/j.agrformet.2015.11.006

Coumou, D., & Rahmstorf, S. (2012). A decade of weather extremes. *Nature Climate Change*, *2*(7), 491–496. https://doi.org/10.1038/nclimate1452

Damour, G., Simonneau, T., Cochard, H., & Urban, L. (2010). An overview of models of stomatal conductance at the leaf level. *Plant, Cell and Environment*, *33*(9), 1419–1438. https://doi.org/10.1111/j.1365-3040.2010.02181.x

De Kauwe, M. G., Zhou, S. X., Medlyn, B. E., Pitman, A. J., Wang, Y. P., Duursma, R. A., & Prentice, I. C. (2015). Do land surface models need to include differential plant species responses to drought? Examining model predictions across a mesic-xeric gradient in Europe. *Biogeosciences*, *12*(24), 7503–7518. https://doi.org/10.5194/bg-12-7503-2015

Ficklin, D. L., & Novick, K. A. (2017). Historic and projected changes in vapor pressure deficit suggest a continental-scale drying of the United States atmosphere. *Journal of Geophysical Research: Atmospheres*, *122*, 2061–2079. https://doi.org/10.1002/2016JD025855

Fischer, E. M., Seneviratne, S. I., Luthi, D., & Schar, C. (2007). Contribution of land-atmosphere coupling to recent European summer heat waves. *Geophysical Research Letters*, *34*, L06707. https://doi.org/10.1029/2006GL029068

Fischer, E. M., Seneviratne, S. I., Vidale, P. L., Luthi, D., & Schar, C. (2007). Soil moisture - Atmosphere interactions during the 2003 European summer heat wave. *Journal of Climate*, *20*(20), 5081–5099. https://doi.org/10.1175/JCLI4288.1

Foken, T. (2008). The energy balance closure problem: An overview. *Ecological Applications*, *18*(6), 1351–1367. https://doi.org/10.1890/06-0922.1

Gentine, P., Entekhabi, D., Chehbouni, A., Boulet, G., & Duchemin, B. (2007). Analysis of evaporative fraction diurnal behaviour. *Agricultural and Forest Meteorology*, *143*(1-2), 13–29. https://doi.org/10.1016/j.agrformet.2006.11.002

Harlan, S. L., Brazel, A. J., Prashad, L., Stefanov, W. L., & Larsen, L. (2006). Neighborhood microclimates and vulnerability to heat stress. *Social Science & Medicine*, *63*(11), 2847–2863. https://doi.org/10.1016/j.socscimed.2006.07.030

Hirschi, M., Seneviratne, S. I., Alexandrov, V., Boberg, F., Boroneant, C., Christensen, O. B., et al. (2011). Observational evidence for soil-moisture impact on hot extremes in southeastern Europe. *Nature Geoscience*, *4*(1), 17–21. https://doi.org/10.1038/ngeo1032

Jarvis, P. G. (1976). The interpretation of the variations in leaf water potential and stomatal conductance found in canopies in the field. *Philosophical Transactions of the Royal Society of London. B, Biological Sciences*, *273*(927), 593–610. https://doi.org/10.1098/rstb.1976.0035

Jones, H. G. (2014). *Plants and microclimate: A quantitative approach to environmental plant physiology* (3rd ed., Vol. xvii, 407 pp). Cambridge, New York: Cambridge University Press.

Konings, A. G., Williams, A. P., & Gentine, P. (2017). Sensitivity of grassland productivity to aridity controlled by stomatal and xylem regulation. *Nature Geoscience*, *10*(4), 284–288. https://doi.org/10.1038/ngeo2903

Kovats, R. S., & Hajat, S. (2008). Heat stress and public health: A critical review. *Annual Review of Public Health*, *29*(1), 41–55. https://doi.org/10.1146/annurev.publhealth.29.020907.090843

Lau, N. C., & Nath, M. J. (2012). A model study of heat waves over North America: Meteorological aspects and projections for the twenty-first century. *Journal of Climate*, *25*(14), 4761–4784. https://doi.org/10.1175/JCLI-D-11-00575.1

Lau, N. C., & Nath, M. J. (2014). Model simulation and projection of European heat waves in present-day and future climates. *Journal of Climate*, *27*(10), 3713–3730. https://doi.org/10.1175/JCLI-D-13-00284.1

Lemordant, L., Gentine, P., Stefanon, M., Drobinski, P., & Fatichi, S. (2016). Modification of land-atmosphere interactions by CO_2 effects: Implications for summer dryness and heat wave amplitude. *Geophysical Research Letters*, *43*, 10,240–10,248. https://doi.org/10.1002/2016GL069896

Li, D., & Bou-Zeid, E. (2013). Synergistic interactions between urban heat islands and heat waves: The impact in cities is larger than the sum of its parts. *Journal of Applied Meteorology and Climatology*, *52*(9), 2051–2064. https://doi.org/10.1175/JAMC-D-13-02.1

Li, D., Liao, W., Rigden, A. J., Liu, X., Wang, D., Malyshev, S., & Shevliakova, E. (2019). Urban heat island: Aerodynamics or imperviousness? *Science Advances*, *5*(4), eaau4299. https://doi.org/10.1126/sciadv.aau4299

Li, D., Sun, T., Liu, M. F., Yang, L., Wang, L., & Gao, Z. Q. (2015). Contrasting responses of urban and rural surface energy budgets to heat waves explain synergies between urban heat islands and heat waves. *Environmental Research Letters*, *10*(5), 054009. https://doi.org/10.1088/1748-9326/10/5/054009

Liao, W. L., Rigden, A. J., & Li, D. (2018). Attribution of local temperature response to deforestation. *Journal of Geophysical Research: Biogeosciences*, *123*, 1572–1587. https://doi.org/10.1029/2018JG004401

Massmann, A., Gentine, P., & Lin, C. J. (2018). When does vapor pressure deficit drive or reduce evapotranspiration? Hydrology and Earth System Sciences Discussions. https://doi.org/10.5194/hess-2018-553

Meehl, G. A., & Tebaldi, C. (2004). More intense, more frequent, and longer lasting heat waves in the 21st century. *Science*, *305*(5686), 994–997. https://doi.org/10.1126/science.1098704

Miralles, D. G., Gentine, P., Seneviratne, S. I., & Teuling, A. J. (2018). Land–atmospheric feedbacks during droughts and heatwaves: State of the science and current challenges. *Annals of the New York Academy of Sciences*, *1436*(1), 19–35. https://doi.org/10.1111/nyas.13912

Miralles, D. G., Teuling, A. J., van Heerwaarden, C. C., & de Arellano, J. V. G. (2014). Mega-heatwave temperatures due to combined soil desiccation and atmospheric heat accumulation. *Nature Geoscience*, *7*(5), 345–349. https://doi.org/10.1038/ngeo2141

Monteith, J. L., & Unsworth, M. H. (2008). *Principles of environmental physics* (3rd ed., Vol. xxi, 418 pp.). Amsterdam; Boston: Elsevier.

Novick, K. A., Ficklin, D. L., Stoy, P. C., Williams, C. A., Bohrer, G., Oishi, A. C., et al. (2016). The increasing importance of atmospheric demand for ecosystem water and carbon fluxes. *Nature Climate Change*, *6*(11), 1023–1027. https://doi.org/10.1038/nclimate3114

Oren, R., Sperry, J. S., Katul, G. G., Pataki, D. E., Ewers, B. E., Phillips, N., & Schafer, K. V. R. (1999). Survey and synthesis of intra- and interspecific variation in stomatal sensitivity to vapour pressure deficit. *Plant, Cell & Environment*, *22*(12), 1515–1526. https://doi.org/10.1046/j.1365-3040.1999.00513.x

Peng, L. Q., Li, D., & Sheffield, J. (2018). Drivers of variability in atmospheric evaporative demand: multiscale spectral analysis based on observations and physically based modeling. *Water Resources Research*, *54*, 3510–3529. https://doi.org/10.1029/2017WR022104

Perkins, S. E. (2015). A review on the scientific understanding of heatwaves—Their measurement, driving mechanisms, and changes at the global scale. *Atmospheric Research*, *164-165*, 242–267. https://doi.org/10.1016/j.atmosres.2015.05.014

Peterson, T. C., Heim, R. R. Jr., Hirsch, R., Kaiser, D. P., Brooks, H., Diffenbaugh, N. S., et al. (2013). Monitoring and understanding changes in heat waves, cold waves, floods, and droughts in the United States: State of knowledge. *Bulletin of the American Meteorological Society*, *94*(6), 821–834. https://doi.org/10.1175/BAMS-D-12-00066.1

Petkova, E. P., Morita, H., & Kinney, P. L. (2014). Health Impacts of heat in a changing climate: how can emerging science inform urban adaptation planning? *Current Epidemiology Reports*, *1*(2), 67–74. https://doi.org/10.1007/s40471-014-0009-1

Rigden, A. J., & Li, D. (2017). Attribution of surface temperature anomalies induced by land use and land cover changes. *Geophysical Research Letters*, *44*, 6814–6822. https://doi.org/10.1002/2017GL073811

Rigden, A. J., & Salvucci, G. D. (2015). Evapotranspiration based on equilibrated relative humidity (ETRHEQ): Evaluation over the continental US. *Water Resources Research*, *51*, 2951–2973. https://doi.org/10.1002/2014WR016072

Rigden, A. J., Salvucci, G. D., Entekhabi, D., & Gianotti, D. J. S. (2018). Partitioning evapotranspiration over the continental United States using weather station data. *Geophysical Research Letters*, *45*, 9605–9613. https://doi.org/10.1029/2018GL079121

Santanello, J. A., Dirmeyer, P. A., Ferguson, C. R., Findell, K. L., Tawfik, A. B., Berg, A., et al. (2018). Land-atmosphere interactions: The LoCo Perspective. *Bulletin of the American Meteorological Society*, *99*(6), 1253–1272. https://doi.org/10.1175/Bams-D-17-0001.1

Santanello, J. A., Peters-Lidard, C. D., Kennedy, A., & Kumar, S. V. (2013). Diagnosing the nature of land-atmosphere coupling: A case study of dry/wet extremes in the US Southern Great Plains. *Journal of Hydrometeorology*, *14*(1), 3–24. https://doi.org/10.1175/JHM-D-12-023.1

Santanello, J. A., Peters-Lidard, C. D., & Kumar, S. V. (2011). Diagnosing the Sensitivity of local land-atmosphere coupling via the soil moisture-boundary layer interaction. *Journal of Hydrometeorology*, *12*(5), 766–786. https://doi.org/10.1175/JHM-D-10-05014.1

Santanello, J. A., Peters-Lidard, C. D., Kumar, S. V., Alonge, C., & Tao, W. K. (2009). A modeling and observational framework for diagnosing local land-atmosphere coupling on diurnal time scales. *Journal of Hydrometeorology*, *10*(3), 577–599. https://doi.org/10.1175/2009JHM1066.1

Seneviratne, S. I., Corti, T., Davin, E. L., Hirschi, M., Jaeger, E. B., Lehner, I., et al. (2010). Investigating soil moisture-climate interactions in a changing climate: A review. *Earth-Science Reviews*, *99*(3-4), 125–161. https://doi.org/10.1016/j.earscirev.2010.02.004

Seneviratne, S. I., Luthi, D., Litschi, M., & Schar, C. (2006). Land-atmosphere coupling and climate change in Europe. *Nature*, *443*(7108), 205–209. https://doi.org/10.1038/nature05095

Smith, T. T., Zaitchik, B. F., & Gohlke, J. M. (2013). Heat waves in the United States: definitions, patterns and trends. *Climate Change*, *118*(3-4), 811–825. https://doi.org/10.1007/s10584-012-0659-2

Stap, L. B., van den Hurk, B. J. J. M., van Heerwaarden, C. C., & Neggers, R. A. J. (2014). Modeled contrast in the response of the surface energy balance to heat waves for forest and grassland. *Journal of Hydrometeorology*, *15*(3), 973–989. https://doi.org/10.1175/Jhm-D-13-029.1

Stewart, J. B. (1988). Modeling surface conductance of pine forest. *Agricultural and Forest Meteorology*, *43*(1), 19–35. https://doi.org/10.1016/0168-1923(88)90003-2

Tao, Z., Santanello, J. A., Chin, M., Zhou, S., Tan, Q., Kemp, E. M., & Peters-Lidard, C. D. (2013). Effect of land cover on atmospheric processes and air quality over the continental United States—A NASA Unified WRF (NU-WRF) model study. *Atmospheric Chemistry and Physics*, *13*(13), 6207–6226. https://doi.org/10.5194/acp-13-6207-2013

Teuling, A. J., Seneviratne, S. I., Stöckli, R., Reichstein, M., Moors, E., Ciais, P., et al. (2010). Contrasting response of European forest and grassland energy exchange to heatwaves. *Nature Geoscience*, *3*(10), 722–727. https://doi.org/10.1038/ngeo950

Thompson, S. E., Harman, C. J., Konings, A. G., Sivapalan, M., Neal, A., & Troch, P. A. (2011). Comparative hydrology across AmeriFlux sites: The variable roles of climate, vegetation, and groundwater. *Water Resources Research*, *47*, W00J07. https://doi.org/10.1029/2010WR009797

Tyree, M. T., & Sperry, J. S. (1989). Vulnerability of xylem to cavitation and embolism. *Annual Review of Plant Physiology*, *40*(1), 19–36. https://doi.org/10.1146/annurev.pp.40.060189.000315

van Heerwaarden, C. C., & Teuling, A. J. (2014). Disentangling the response of forest and grassland energy exchange to heatwaves under idealized land-atmosphere coupling. *Biogeosciences*, *11*(21), 6159–6171. https://doi.org/10.5194/bg-11-6159-2014

Wolf, S., Eugster, W., Ammann, C., Hani, M., Zielis, S., Hiller, R., et al. (2014). Contrasting response of grassland versus forest carbon and water fluxes to spring drought in Switzerland (vol 8, 035007, 2013). *Environmental Research Letters*, *9*(8). https://doi.org/10.1088/1748-9326/9/8/089501